







## Article

# Impact of Anchoring Groups on the Photocatalytic Performance of Iridium(III) Complexes and Their Toxicological Analysis

 Xiao Yao <sup>1,\*</sup> , Linyu Fan <sup>2,3</sup> , Qian Zhang <sup>2,3</sup> , Chaoqun Zheng <sup>1,\*</sup> , Xue Yang <sup>1</sup>, Yisang Lu <sup>1</sup>   
 and Yachen Jiang <sup>1</sup> 
<sup>1</sup> School of Ecological Environment and Urban Construction, Fujian University of Technology, Fuzhou 350118, China

<sup>2</sup> Department of Applied Biology and Chemical Technology, The Hong Kong Polytechnic University, Hung Hom, Hong Kong, China

<sup>3</sup> PolyU Shenzhen Research Institute, Shenzhen 518057, China

\* Correspondence: 18041778r@connect.polyu.hk (X.Y.); panpantiao@163.com (C.Z.)

**Abstract:** Three different iridium(III) complexes, labelled as Ir1–Ir3, each bearing a unique anchoring moiety (diethyl [2,2′-bipyridine]-4,4′-dicarboxylate, tetraethyl [2,2′-bipyridine]-4,4′-diylbis(phosphonate), or [2,2′-biquinoline]-4,4′-dicarboxylic acid), were synthesized to serve as photosensitizers. Their electrochemical and photophysical characteristics were systematically investigated. ERP measurements were employed to elucidate the impact of the anchoring groups on the photocatalytic hydrogen generation performance of the complexes. The novel iridium(III) complexes were integrated with platinumized TiO<sub>2</sub> (Pt–TiO<sub>2</sub>) nanoparticles and tested for their ability to catalyze hydrogen production under visible light. A H<sub>2</sub> turnover number (TON) of up to 3670 was obtained upon irradiation for 120 h. The complexes with tetraethyl [2,2′-bipyridine]-4,4′-diylbis(phosphonate) anchoring groups were found to outperform those bearing other moieties, which may be one of the important steps in the development of high-efficiency iridium(III) photosensitizers for hydrogen generation by water splitting. Additionally, toxicological analyses found no significant difference in the toxicity to luminescent bacteria of any of the present iridium(III) complexes compared with that of TiO<sub>2</sub>, which implies that the complexes investigated in this study do not pose a high risk to the aquatic environment compared to TiO<sub>2</sub>.

**Keywords:** Ir(III) cyclometalated; anchoring ligand; carbazole; photosensitizers; biquinoline



**Citation:** Yao, X.; Fan, L.; Zhang, Q.; Zheng, C.; Yang, X.; Lu, Y.; Jiang, Y. Impact of Anchoring Groups on the Photocatalytic Performance of Iridium(III) Complexes and Their Toxicological Analysis. *Molecules* **2024**, *29*, 2564. <https://doi.org/10.3390/molecules29112564>

Academic Editor: Hristiyan A. Aleksandrov

Received: 18 April 2024

Revised: 20 May 2024

Accepted: 28 May 2024

Published: 30 May 2024



**Copyright:** © 2024 by the authors. Licensee MDPI, Basel, Switzerland. This article is an open access article distributed under the terms and conditions of the Creative Commons Attribution (CC BY) license (<https://creativecommons.org/licenses/by/4.0/>).

## 1. Introduction

In light of the increasing demand for energy and diminishing global fossil fuel supply, the quest for alternative energy sources has evolved into a critical and intricate field of research [1]. Solar power surfaced as a viable solution to contemporary energy challenges owing to its sustainability and zero-carbon footprint [2]. Photocatalytic technology enables the effective harnessing and conversion of this energy type into various forms of power [3–10]. Particularly, the solar-driven photocatalytic water splitting technique offers an easy procedure for producing hydrogen fuel [11,12], a concept initially introduced in 1972 by Fujishima and Honda by utilising a TiO<sub>2</sub> photoanode [13]. After this study, the technology for hydrogen production through water splitting has evolved significantly [14,15].

Iridium(III) cyclometalated complexes, distinguished for their role in dye fabrication, have significantly contributed to the field of photocatalytic hydrogen production [16]. These complexes are essential for their superior ligand-field stabilisation energy, primarily attributed to the 5d valence shell, especially when compared with other metal dyes derived from first- and second-row transition metals [2,17]. Research led by Bernhard et al. [2,18–20] has explored the potential of iridium(III) complexes, particularly those following the formula [Ir(C^N)<sub>2</sub>(N^N)]<sup>+</sup> (where C^N represents the cyclometalating ligand and N^N denotes the anchoring group), in applications related to photochemical water splitting for

hydrogen production. Impressive results, such as a turnover number (TON) of 800, were achieved utilizing 50  $\mu\text{M}$  of  $[\text{Ir}(\text{ppy})_2(\text{bpy})]^+$  as a photosensitizer within a water–acetonitrile solvent mixture at a ratio of 1:1 (*v/v*) [18,21–24]. Subsequently, Ir(III) cyclometalated complexes have garnered interest for their potential applications as photosensitizers [25–27]. The stability of these complexes is enhanced through C^N ligands, which provide  $\sigma$ -donation from carbon atoms bonded to the metal, increasing electron density at the metal core and improving resilience during photocatalytic experiments [2,28]. Furthermore, physicochemical properties, including energy gaps, can be effectively tuned by varying the ligands [29,30], making Ir(III) cyclometalated complexes attractive candidates for dyes in  $\text{H}_2$  production through water splitting.

However, Ir(III) cyclometalated complexes often demonstrate weak visible light absorption, constituting approximately 40% of the sunlight spectrum [26,30–34]. Adjustments to the structures of Ir(III) cyclometalated complexes are necessary to overcome these limitations and enhance their hydrogen output. The potential for enhancing hydrogen evolution performance in iridium-based photosensitizers remains unexplored. Despite their potential, developing efficient and stable Ir(III) photosensitizers remains crucial for improving the kinetics of hydrogen production. Recent advancements in the field of Ir(III) photosensitizers focus on altering the structure of cyclometalating and ancillary ligands to modify their photochemical and physical attributes [3,16,35,36]. Strategic choices in chromophores and molecular structures can enhance light absorption, electron transfer efficiency, and photosensitizer longevity [37]. Optimizing the donor groups on cyclometalating ligands in Ir(III) photosensitizers enhances spectral responses, accelerates charge transfer, increases stability, and ensures better energy level alignment with  $\text{TiO}_2$  conduction band edges, thereby boosting photocatalytic hydrogen production efficacy [38]. Carbazole (Cz), especially 9-phenyl-9H-carbazole, has been widely used in the synthesis of conjugated microporous polymers for photocatalysis owing to its excellent electron-donating and charge-transporting properties and its suitability for post-functionalization [39,40]. The isoquinoline functional groups have also found extensive application in dyes for water-splitting reactions owing to their significant charge transfer ability [41]. Combining Cz with furan and isoquinoline to form a donor– $\pi$ –acceptor (D– $\pi$ –A) framework enhances strong intramolecular charge transfer (ICT) capabilities, resulting in high molar extinction coefficients in the resultant iridium(III) complexes [42,43].

Previous studies on Ir(III) cyclometalated complexes have found that different anchoring groups on N^N ligands are used to achieve highly efficient and stable water-splitting systems [44,45]. Incorporating anchoring groups, including carboxylate, or phosphonic acid, into the bipyridine ligand structure of  $[\text{Ir}(\text{C}^{\text{N}})_2(\text{N}^{\text{N}})]^+$ -type dyes [45] facilitates their stable attachment to semiconductors. The presence of a 2,2'-bipyridine or biquinoline moiety in these anchoring groups significantly enhances the molar extinction coefficients of these complexes, thereby increasing their light absorption capacity, which is crucial for photocatalytic water splitting to generate hydrogen [46]. Complexes with carboxyl functional groups on their anchoring ligands establish strong connections with semiconductors such as  $\text{TiO}_2$ . This results in improved electron transport and hydrogen production and increased water solubility due to the acid–base equilibrium in Ir(III) cyclometalated complexes [47–50]. However, the stability of these dyes under photocatalytic conditions may pose a challenge [51], with the hydrolysis of carboxylate linkages identified as a limiting factor in the efficiency of electron transfer from the photosensitizer to the  $\text{TiO}_2$  surface [52]. In contrast, phosphonate linkages demonstrate enhanced stability when bonded to  $\text{TiO}_2$  surfaces, surpassing the performance of carboxylate linkages [26,52].

Three Ir(III) complexes have been synthesized, denoted as **Ir1** to **Ir3**. These complexes feature diethyl [2,2'-bipyridine]-4,4'-dicarboxylate, tetraethyl [2,2'-bipyridine]-4,4'-diylbis(phosphonate), or [2,2'-Biquinoline]-4,4'-dicarboxylic acid as anchoring units. They are designed to serve as photosensitizers in light-driven hydrogen production through water splitting (Figure 1). The dye molecular structure includes 3-(5-(isoquinolin-1-yl)furan-2-yl)-9-phenyl-9H-carbazole motifs, forming a donor– $\pi$ –acceptor (D– $\pi$ –A) architecture [42,43,53–56].

Furthermore,  $[\text{Ir}(\text{ppy})_2(\text{dcbpy})]\text{Cl}$  was synthesized to serve as a benchmark for evaluating the light-harvesting abilities and hydrogen generation efficiency of these synthesized dyes. Therefore, this study aims to investigate the effect of the C<sup>∞</sup>N ligands and anchoring units on the properties of these complexes through a comprehensive analysis employing both electrochemical and photophysical techniques. Furthermore, systematic investigations into their photocatalytic hydrogen production capabilities through water splitting were undertaken, including exploring the correlation between the anchoring groups and their hydrogen generation activities. Additionally, toxicology research was conducted to check their environmental influence.

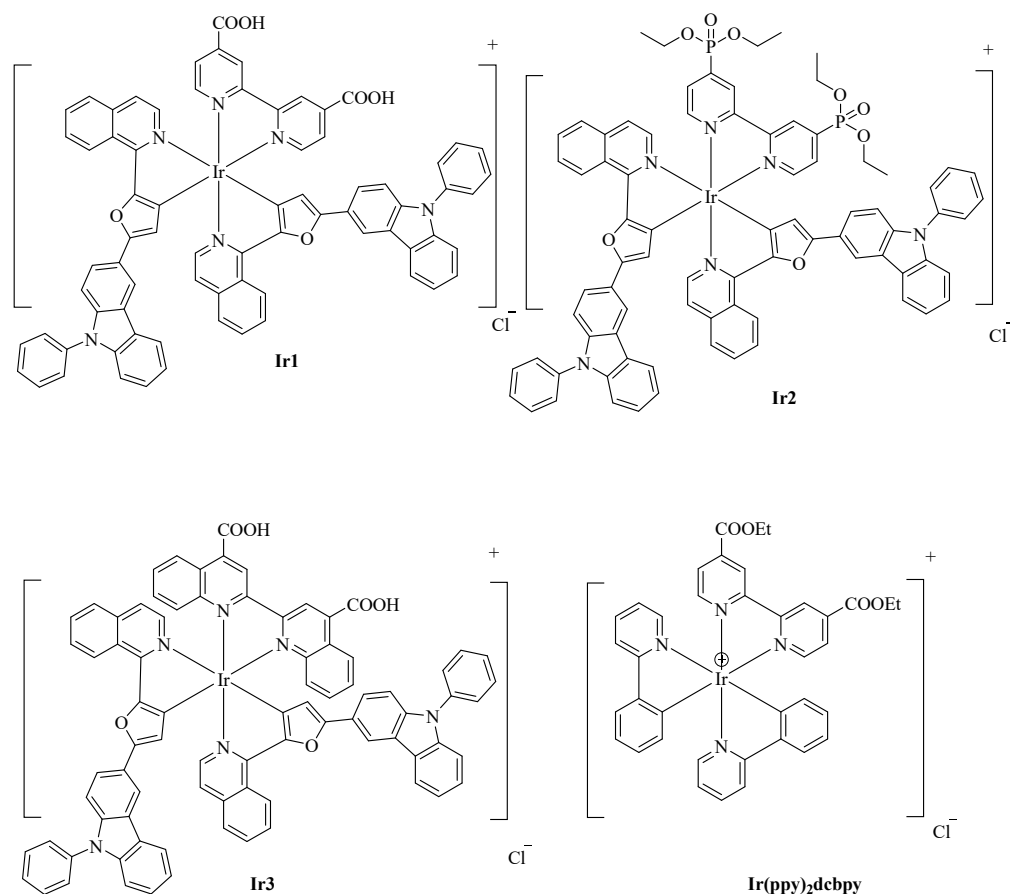
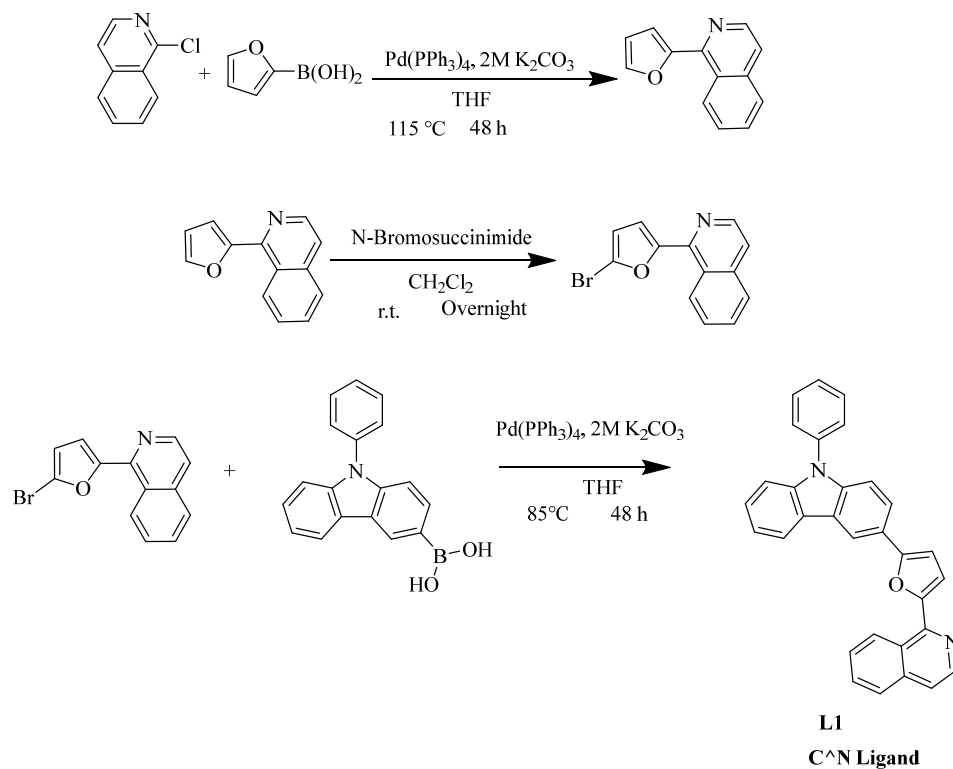


**Figure 1.** Chemical structures of iridium(III) dyes **Ir1–Ir3** and  $[\text{Ir}(\text{ppy})_2(\text{dcbpy})]\text{Cl}$ .

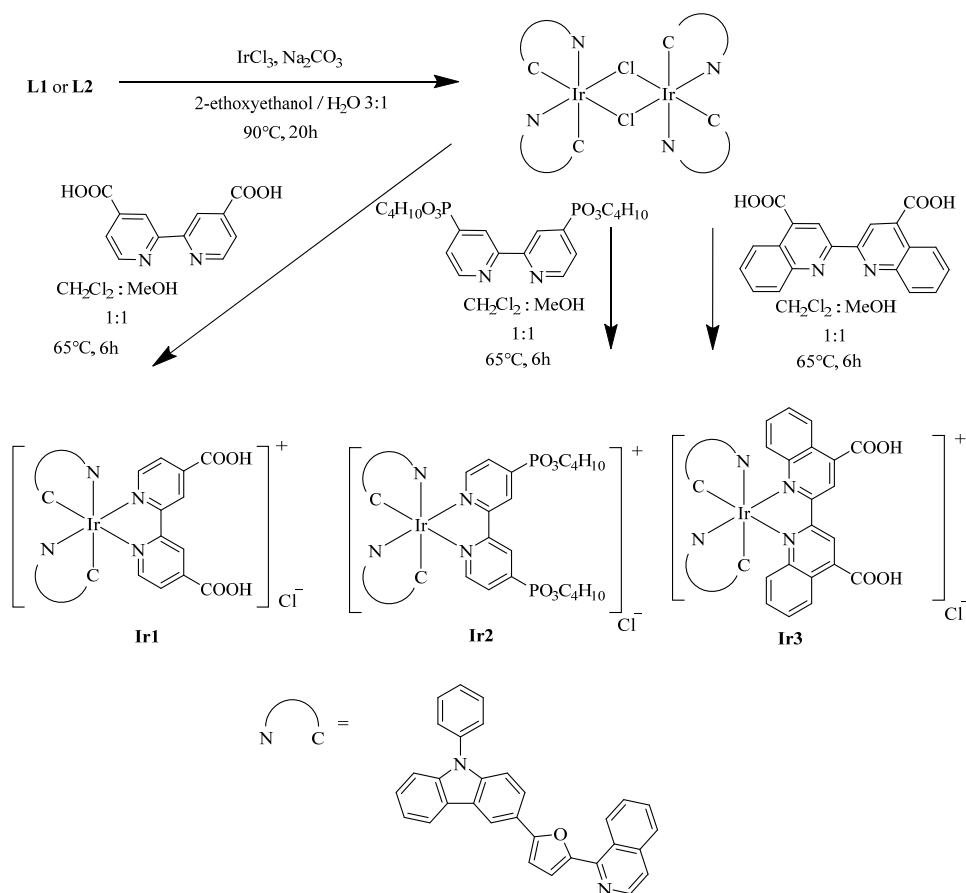
## 2. Results and Discussion

### 2.1. Synthesis and Characterization

Schemes 1 and 2 illustrate the synthetic methodologies for the C<sup>∞</sup>N ligands and Ir(III) photosensitizers, respectively. Photosensitizers structure consists of an Ir(III) core surrounded by two C<sup>∞</sup>N cyclometalating ligands and a variable N<sup>∞</sup>N auxiliary ligand, which is diethyl [2,2'-bipyridine]-4,4'-dicarboxylate, tetraethyl [2,2'-bipyridine]-4,4'-diylbis(phosphonate), or [2,2'-Biquinoline]-4,4'-dicarboxylic acid. The C<sup>∞</sup>N ligand was synthesized utilizing the Suzuki coupling reaction. For Ir(III) complexes (**Ir1–Ir3**) generation, a two-stage synthetic strategy was employed. Initially,  $\mu$ -chloride-bridged dimeric complexes were synthesized by reacting Ir(III) chloride hydrate with the C<sup>∞</sup>N cyclometalating ligand [57,58]. These dimers were subsequently reacted with the N<sup>∞</sup>N auxiliary ligands to form the final Ir(III) complexes (**Ir1–Ir3**). These Ir(III) complexes demonstrate stability as solid substances under atmospheric conditions.



Scheme 1. Synthetic route for cyclometalating ligand.



Scheme 2. Synthetic route for iridium(III) complexes Ir1–Ir3.

All synthesized organic precursors and ligands underwent characterization using  $^1\text{H}$  and  $^{13}\text{C}$  NMR spectroscopic techniques. Additionally, a comprehensive analysis of the Ir(III) complexes was performed utilizing a combination of LC-ESI-Q-TOF MS and  $^1\text{H}$  NMR spectroscopy. A distinct peak observed between approximately 8.74 to 9.28 ppm in the  $^1\text{H}$  NMR spectra is attributed to the ortho proton of isoquinoline [11]. These spectroscopic findings corroborate the anticipated molecular structures of the complexes. However, obtaining high-quality  $^{13}\text{C}$  NMR spectra proved challenging owing to the complex limited solubility in commonly used organic solvents.

## 2.2. Photophysical Properties of Iridium(III) Dyes

The photophysical characteristics of Ir(III) complexes were investigated in dichloromethane at ambient temperature (293 K). Table 1 lists their unique UV/Vis absorption spectra, while Figure 2 graphically represents them. Ir1 to Ir3 demonstrates significant absorption of approximately 230 nm in the UV region, which is attributed to intra-ligand charge transfer transitions [59]. The prominent band observed at approximately 400 nm is owing to spin-allowed  $\pi$  to  $\pi^*$  electronic transitions within the C $\wedge$ N and N $\wedge$ N ligands [36]. Both metal-to-ligand charge transfer (MLCT) and ligand-to-ligand charge transfer (LLCT) contribute to the extensive absorption bands observed around 400 nm [60]. These compounds demonstrated superior absorption intensity in the visible spectrum than in the conventional  $[\text{Ir}(\text{ppy})_2(\text{dcbpy})]\text{Cl}$  complex, indicating enhanced light-harvesting efficiency in Ir1–Ir3 over  $[\text{Ir}(\text{ppy})_2(\text{dcbpy})]\text{Cl}$  [30,61,62]. The broadened absorption spectra with higher  $\epsilon$  values in 500 nm range result from the extended  $\pi$ -conjugation provided by the electron-donating Cz group in the Ir(III) dyes [63]. In addition, Ir3 showed a slight redshift with lower molar absorptivity compared to Ir1, possibly owing to the extension of conjugation in the anchoring group [39].

**Table 1.** UV–Vis absorption parameter values of Ir1 to Ir3 in  $\text{CH}_2\text{Cl}_2$  at 293 K.

Dye	$\lambda_{\text{max}}/\text{nm}$ ( $\epsilon/10^5 \text{ M}^{-1} \text{ cm}^{-1}$ )	$\lambda_{\text{onset}}/\text{nm}$
Ir1	234 (5.45), 280 (2.64), 490 (0.96)	597
Ir2	233 (5.36), 278 (2.64), 306 (2.43), 497 (1.07)	574
Ir3	237 (4.91), 283 (2.51), 492 (0.84)	601
$[\text{Ir}(\text{ppy})_2(\text{dcbpy})]\text{Cl}$	240 (2.64), 311 (0.86), 340 (0.52), 398 (0.12)	427

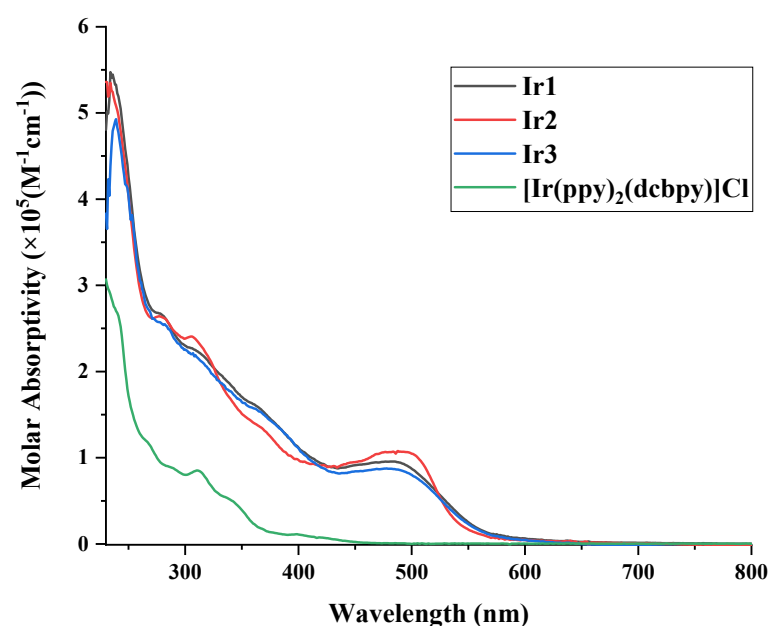


**Figure 2.** UV–Vis absorption spectra of Ir1 to Ir3 and  $[\text{Ir}(\text{ppy})_2(\text{dcbpy})]\text{Cl}$  in  $\text{CH}_2\text{Cl}_2$  at 293 K.

Figure 3 presents the photoluminescence profiles of Ir1 to Ir3 in a dichloromethane solution at 293 K. Upon photochemical excitation at 480 nm, distinct emission spectra are observed for all Ir(III) dyes. These emissions originate from a combination of  $^3\text{MLCT}$  and  $\text{LC } ^3\pi$  to  $\pi^*$  transitions [64–66]. The photoluminescence spectra of Ir1 and Ir3 demonstrate only negligible change, indicating the same energy levels. This observation is consistent with the electrochemical data.

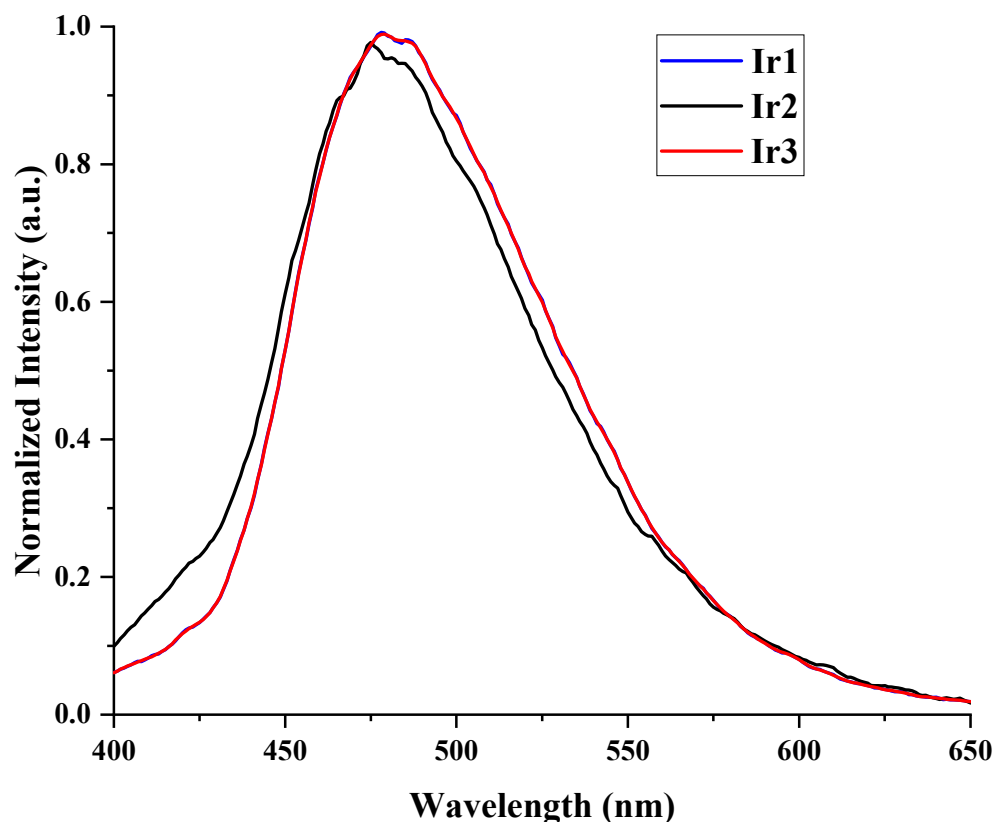


Figure 3. PL spectra of Ir1–Ir3 in dichloromethane solution at 293 K.

### 2.3. Electrochemical Properties of Iridium(III) Dyes

Optimizing the energy gap between the  $\text{TiO}_2$  semiconductor and sacrificial electron donor in Ir(III) complexes is crucial for efficient hydrogen production through water splitting. Electron transfer efficacy and charge separation in these complexes depends on the LUMO energy level being higher than the conduction band of the semiconductor and the HOMO level being below the sacrificial electron donor. To elucidate the energy profiles of the Ir(III) complexes, cyclic voltammetry (CV) was employed utilizing a standard three-electrode set-up. Table 2 summarizes the comprehensive parameters derived from these experiments.

Table 2. Electrochemical data and energy levels of Ir1–Ir3.

Dye	$E_{\text{Ox}}^{\text{Max}}/\text{V}$	$E_{\text{HOMO}}^{\text{[a]}}/\text{eV}$	$E_{\text{g}}^{\text{[b]}}/\text{eV}$	$E_{\text{LUMO}}^{\text{[c]}}/\text{eV}$
Ir1	0.86	−5.66	2.07	−3.59
Ir2	0.85	−5.65	2.16	−3.49
Ir3	0.86	−5.66	2.06	−3.60
$[\text{Ir}(\text{ppy})_2(\text{dcbpy})]\text{Cl}$	1.39	−6.19	2.90	−3.29

<sup>[a]</sup> Calculated as  $-(E_{\text{Ox}}^{\text{Max}} + 4.8)$ . <sup>[b]</sup> Energy band gap, determined from the onset of absorption.

<sup>[c]</sup>  $E_{\text{LUMO}} = E_{\text{HOMO}} + E_{\text{g}}$ .

The CV results demonstrated significant differences compared to those obtained for  $[\text{Ir}(\text{ppy})_2(\text{dcbpy})]\text{Cl}$ , indicating that the different ligands significantly influenced the energy

gaps in Ir(III) dyes [29,30]. The CV data indicate that the conduction band of the TiO<sub>2</sub> semiconductor, at  $-4.4$  eV, was lower than the  $E_{\text{LUMO}}$  levels of all Ir(III) dyes, ranging from  $-3.60$  to  $-3.49$  eV. This difference facilitates effective electron injection during light-induced hydrogen production [67]. The  $E_{\text{HOMO}}$  values of **Ir1–Ir3** were  $-5.66$  or  $-5.65$  V, which was more negative than the redox potentials of the sacrificial electron donor (AA) ( $-4.65$  eV, pH $\sim$ 4) [68,69], thereby enabling effective dye regeneration from the sacrificial electron donor. All the Ir(III) dyes demonstrated energy levels that meet the prerequisites for efficient electron injection and charge separation, highlighting their potential suitability for hydrogen production through water splitting.

Previous research indicates that the HOMO energy levels are primarily located at the Ir centre and on cyclometalating C^N ligands and can be readily adjusted. In contrast, the LUMO energy levels are distributed across the anchoring N^N groups [26,57]. The phosphonate anchoring groups establish a stronger chemical linkage to the TiO<sub>2</sub> surface, thereby tuning the LUMO energy level and enhancing the water-splitting hydrogen generation [45]. The energy level of **Ir1** and **Ir3** are quite the same, as predicted by PL data previously (Figure 3).

#### 2.4. Electrochemical Impedance Spectroscopy (EIS) of Iridium(III) Dyes

To investigate the charge recombination properties of Ir(III) complexes, EIS was utilized [70,71]. Figure 4 shows the EIS Nyquist plots for **Ir1** to **Ir3**. It is well-established that a smaller arc radius on the EIS Nyquist plot indicates reduced resistance to electrical charge transfer, thereby enhancing hydrogen production performance [70–73]. **Ir2** demonstrated the smallest arc radius among the dyes, signifying its superior charge carrier transfer capabilities [74]. These observations are consistent with the hydrogen production efficiency of the dyes in water-splitting processes.

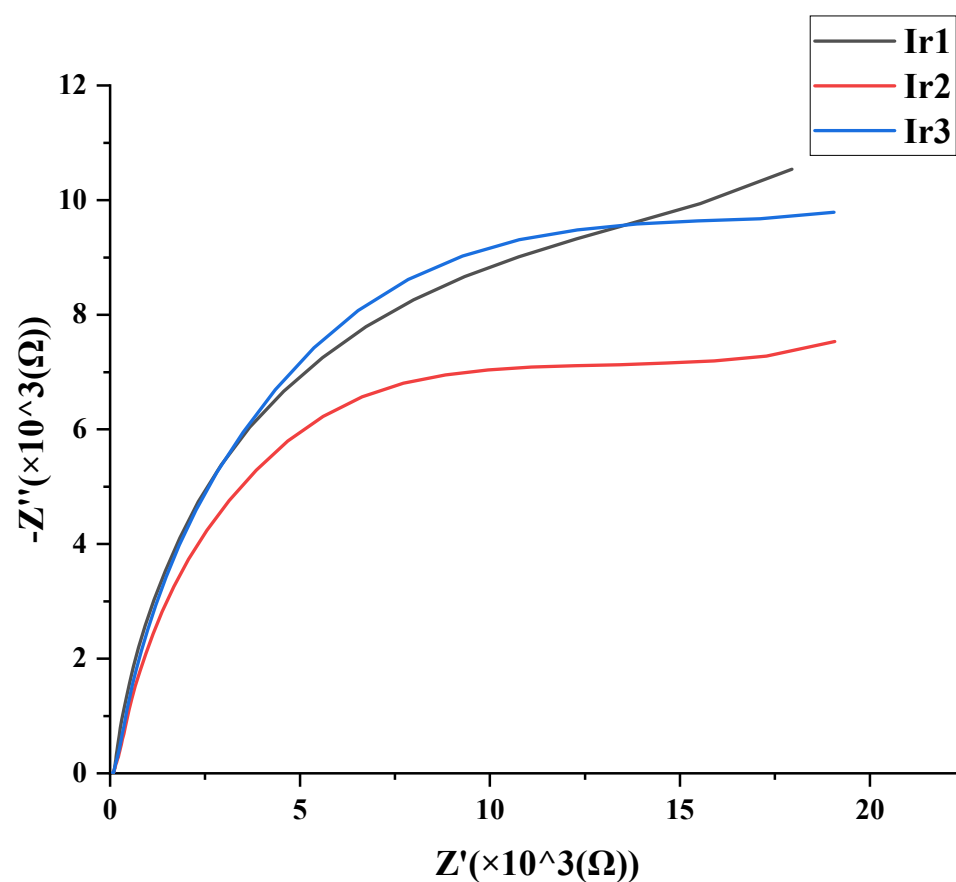


Figure 4. EIS Nyquist plots for complexes **Ir1–Ir3**.

### 2.5. Photocurrent Measurements of Iridium(III) Dyes

Photocurrent measurements were utilized to assess the stability and efficiency of charge separation in the metal complexes [75]. Consistent and rapid photocurrent response in light-on/light-off tests signifies steady photocatalytic activity [76] while heightened photocurrent density indicates efficient charge separation [77]. The photocurrent testing followed a previously established methodology [78]. Figure 5 illustrates the photocurrent behaviour of Ir1–Ir3 under cycles of visible light exposure, depicting six on–off cycles. This clearly demonstrates efficient electron transfer [78], indicative of their consistent photocatalytic performance [76]. Ir2 demonstrated a substantially increased photocurrent intensity when illuminated and a pronounced setback in its decrease upon light-off. This suggests greater efficiency in charge separation and an enhanced ability for hydrogen production compared to other dyes [76,78–80].

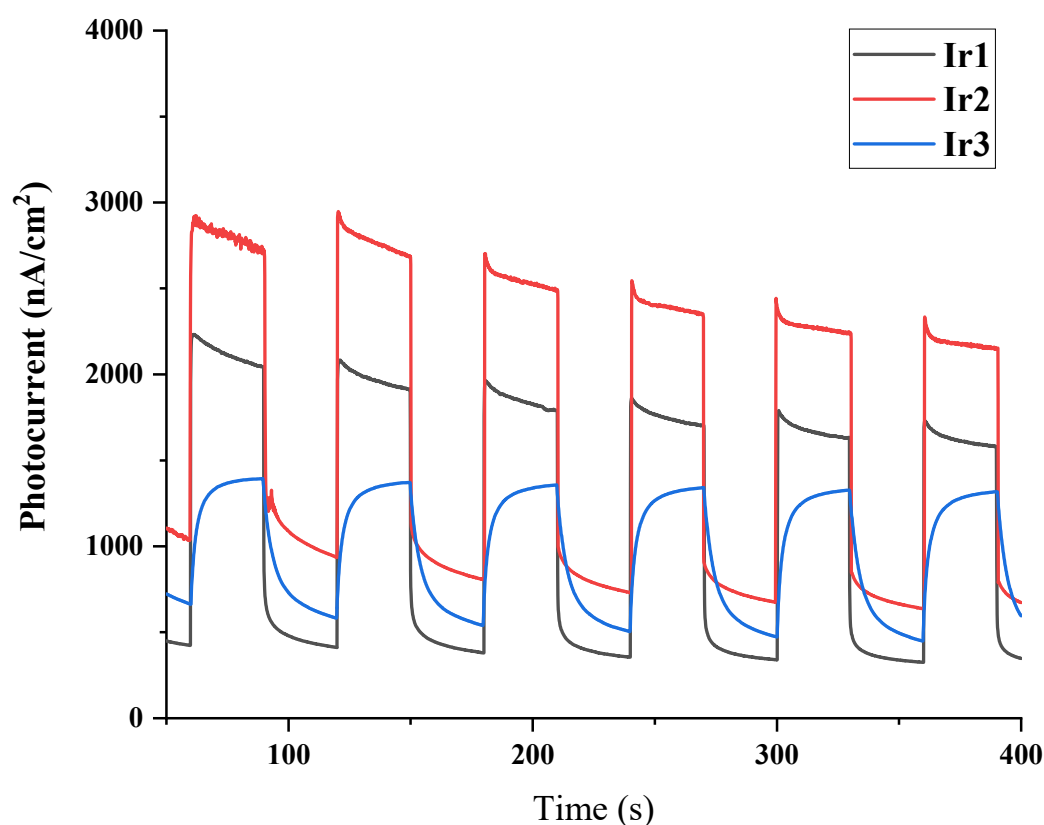


Figure 5. The photocurrent responses of Ir1–Ir3.

### 2.6. Electron Paramagnetic Resonance (EPR) Studies of Ir@Pt-TiO<sub>2</sub>

In this photocatalytic process, the photosensitizer is photoexcited under light irradiation, leading to electron transfer to the conduction band of TiO<sub>2</sub>. The photo-generated electrons and holes can undergo recombination in bulk or on the surface of the semiconductor very quickly, releasing energy in the form of heat or photons. These unreacted electrons are then relayed to Pt nanoparticles on the TiO<sub>2</sub> surface, facilitating proton reduction and hydrogen release. Electron paramagnetic resonance was conducted to Ir2@Pt-TiO<sub>2</sub> and Ir1@Pt-TiO<sub>2</sub> (Figure 6). It is well known that as more electrons are produced, TEMPO<sup>+</sup> is increasingly reduced, and as the amount of detectable TEMPO<sup>+</sup> decreases, the signal decreases [81]. It can be inferred that, by observing the increased generation of photo-generated electrons by Ir2@Pt-TiO<sub>2</sub>, it is reasonable to anticipate that it will exhibit a higher efficiency in hydrogen production [82].



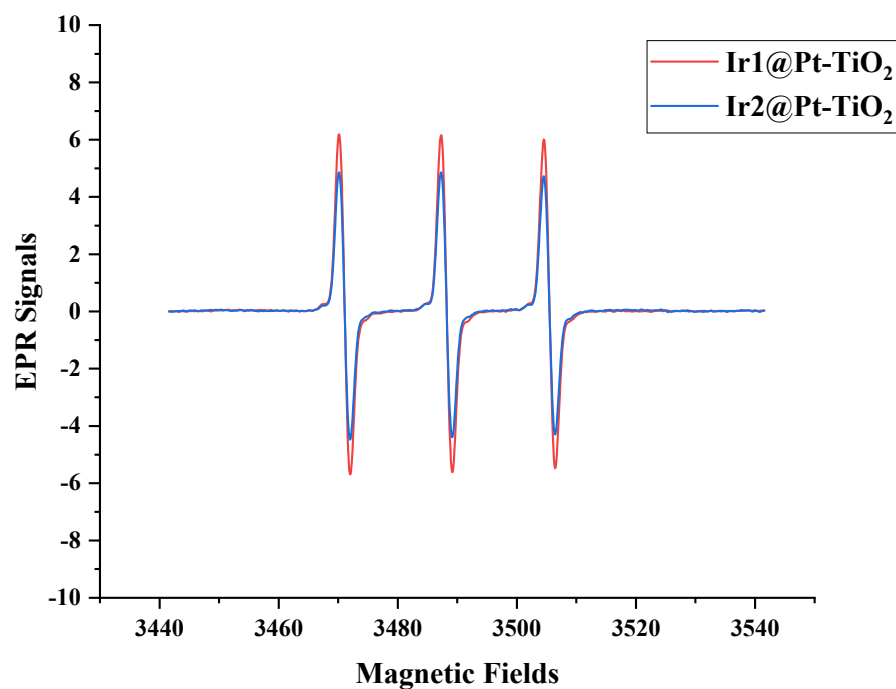


Figure 6. EPR results of Ir1@Pt-TiO<sub>2</sub> and Ir2@Pt-TiO<sub>2</sub>.

### 2.7. Light-Driven Hydrogen Generation Studies of Ir@Pt-TiO<sub>2</sub>

The process of hydrogen generation through water splitting involved the use of Ir(III) complexes as photosensitizers. Detailed procedures for synthesizing platinized TiO<sub>2</sub>, conjugating Ir(III) complexes to the platinized TiO<sub>2</sub>, and executing the photocatalytic water-splitting process, are provided in the experimental section. Generally, each Ir(III) complex was bonded to the platinized TiO<sub>2</sub> utilizing a sonication technique. Subsequently, the mixture underwent centrifugation and drying before the water-splitting experiment. Dye coupling effectiveness for each specimen was assessed by measuring absorbance shifts at the absorption peaks before and post-dye application, indicating a dyeing efficiency of approximately 100%.

Photocatalytic water splitting for hydrogen generation was performed in a 5 mL AA solution (0.5 M) at pH 4.0, serving as the sacrificial electron donor. The experimental configuration employed single-neck 25 mL reaction flasks for the photocatalytic processes. Continuous illumination was provided by blue LEDs (470 nm). Hydrogen production from each specimen was qualitatively and quantitatively assessed using gas chromatography, with methane as the internal standard. Figure 7 illustrates the hydrogen production profiles over time for each sample. Table 3 presents relevant data, including TON, turnover frequency (TOF), initial turnover frequency (TOF<sub>i</sub>), and Activity<sub>i</sub>. In this photocatalytic process, the photosensitizer is photoexcited under light irradiation, leading to electron transfer to the conduction band of TiO<sub>2</sub>. These electrons are afterwards relayed to platinum nanoparticles on the TiO<sub>2</sub> surface, facilitating proton reduction and hydrogen release. The oxidized photosensitizer is subsequently regenerated to its ground state by AA [36,57].

Among the tested systems, the Ir2@Pt-TiO<sub>2</sub> system demonstrated the most effective hydrogen generation ability, achieving TON values of 3670. Following closely, the Ir1@Pt-TiO<sub>2</sub> system recorded TON values of 2553. Higher hydrogen production was achieved when using Ir(III) dyes in the phosphonate anchoring group than in the carboxylate anchoring group. This improvement is attributed to the enhanced anchoring ability provided by the phosphonate group [44,83–85], a finding consistent with previous literature [45,51]. The photocatalytic water-splitting experiments for [Ir(ppy)<sub>2</sub>(dcbpy)]Cl were also performed. Figure 7 and Table 3 show the experimental results. The results suggest that our new complexes show higher stability than [Ir(ppy)<sub>2</sub>(dcbpy)]Cl. These findings indicate that our

new Ir(III) dyes, especially with phosphonate anchoring group, are promising candidates for highly stable photocatalytic applications.

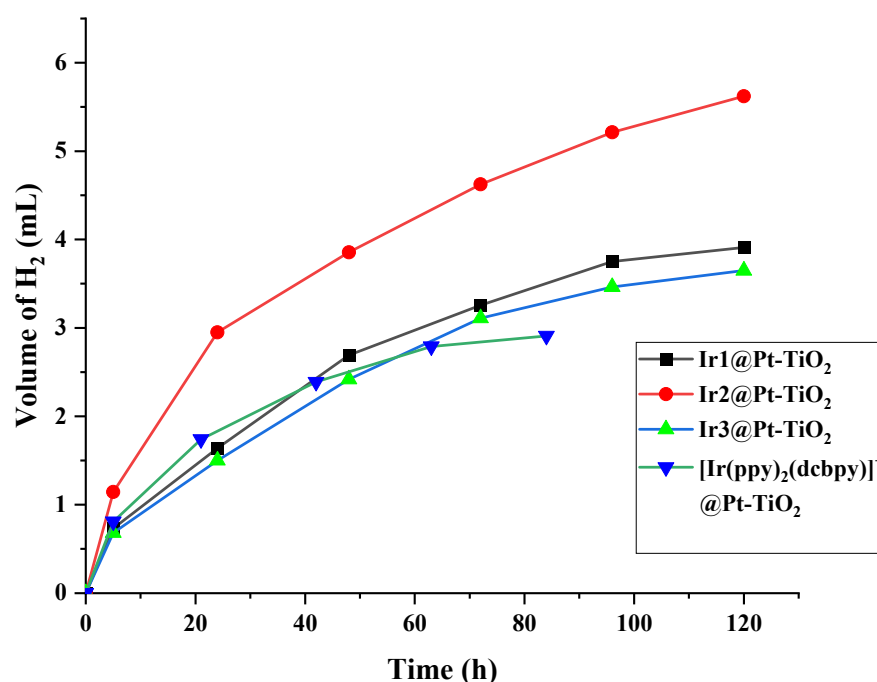


**Figure 7.** Photocatalytic H<sub>2</sub> generation curves of Ir1–Ir3@Pt-TiO<sub>2</sub> and [Ir(ppy)<sub>2</sub>(dcbpy)]<sup>+</sup>@TiO<sub>2</sub> under blue LED irradiation (50 mW).

**Table 3.** Photocatalytic H<sub>2</sub> generation data for different Ir(III) dyes attached to platinized TiO<sub>2</sub> (Ir1–Ir3@Pt-TiO<sub>2</sub>) under blue light irradiation.

Dye	Time/h	H <sub>2</sub> /mL	TON <sup>[a]</sup>	TOF <sup>[b]</sup> /h <sup>-1</sup>	TOF <sub>i</sub> <sup>[c]</sup> /h <sup>-1</sup>	Activity <sub>i</sub> <sup>[d]</sup> /μmol g <sup>-1</sup> h <sup>-1</sup>
Ir1	120	3.91	2553	21.3	95.7	59,810
Ir2	120	5.62	3670	30.6	149.4	93,387
Ir3	120	3.85	2383	19.9	89.0	55,640
[Ir(ppy) <sub>2</sub> (dcbpy)] <sup>+</sup>	84	2.91	1900	22.6	105.8	66,122

<sup>[a]</sup> TON for hydrogen production was determined by doubling the moles of hydrogen generated compared to the moles of photosensitizer bonded to the platinized TiO<sub>2</sub>. <sup>[b]</sup> The TOF of the system was calculated on an hourly basis. <sup>[c]</sup> Initial turnover frequency (TOF<sub>i</sub>) was measured during the first 5 h of the reaction. <sup>[d]</sup> Activity<sub>i</sub> is described as hydrogen quantity (in micromoles) evolved per hour per gram of platinum utilized.

## 2.8. Toxicity Detection of Ir@Pt-TiO<sub>2</sub>

The luminous intensity of luminescent bacteria remains constant under specific conditions but changes upon contact with foreign substances. Within a defined concentration spectrum, the modulation of luminescent intensity correlates directly with toxin concentration. This characteristic facilitates the determination of overall toxicity through comparative assessment of luminous intensity pre- and post-exposure to a substance, employing a dedicated luminescent detector [86]. Several studies have suggested that the toxicity levels of materials can be evaluated through changes in the relative luminous intensity of luminescent bacteria [87–89]. The luminescent intensity was assessed subsequent to the amalgamation of photocatalytic materials with water samples containing luminescent bacilli T3 strain. Moreover, given titanium dioxide's inherent antibacterial properties, it served as the control group in this study. This choice facilitated the computation of relative luminous intensity and enabled the comparative assessment of toxicity levels among various photocatalytic materials [90]. The photocatalytic materials (Ir1@Pt-TiO<sub>2</sub>,

Ir2@Pt-TiO<sub>2</sub>, and Ir3@Pt-TiO<sub>2</sub>) were acquired following a photocatalytic process spanning 0 to 5 days, with subsequent incubation at room temperature for intervals of 0 and 15 min, as illustrated in Figure 8. With an increasing duration of the photocatalytic process, the mean relative luminous intensity of Ir3@Pt-TiO<sub>2</sub> ranged from 104.6% to 120.4%, while for Ir1@Pt-TiO<sub>2</sub> and Ir2@Pt-TiO<sub>2</sub>, it ranged from 81.8% to 114.4%. However, no noteworthy alterations were discerned in the relative luminous intensity of the luminescent bacteria when exposed to the photocatalytic materials (Ir1@Pt-TiO<sub>2</sub>, Ir2@Pt-TiO<sub>2</sub>, and Ir3@Pt-TiO<sub>2</sub>), relative to those exposed to TiO<sub>2</sub>. Traditionally, TiO<sub>2</sub> particles have been viewed as having low solubility and minimal toxicity [91]. These findings suggest that the photocatalytic materials (Ir1@Pt-TiO<sub>2</sub>, Ir2@Pt-TiO<sub>2</sub>, and Ir3@Pt-TiO<sub>2</sub>) do not induce significant toxic effects within the specified timeframe. It is noteworthy that iridium complexes, due to their low toxicity, are commonly utilized in biology and life sciences [92]. Ajay et al. [93] found that iridium exhibits variable oxidation states and dynamic stability in biological systems, making it a viable option as an anticancer drug. Consequently, the photocatalytic materials (Ir1@Pt-TiO<sub>2</sub>, Ir2@Pt-TiO<sub>2</sub>, and Ir3@Pt-TiO<sub>2</sub>) utilized in this investigation do not pose an elevated risk to the aquatic environment compared to TiO<sub>2</sub>.

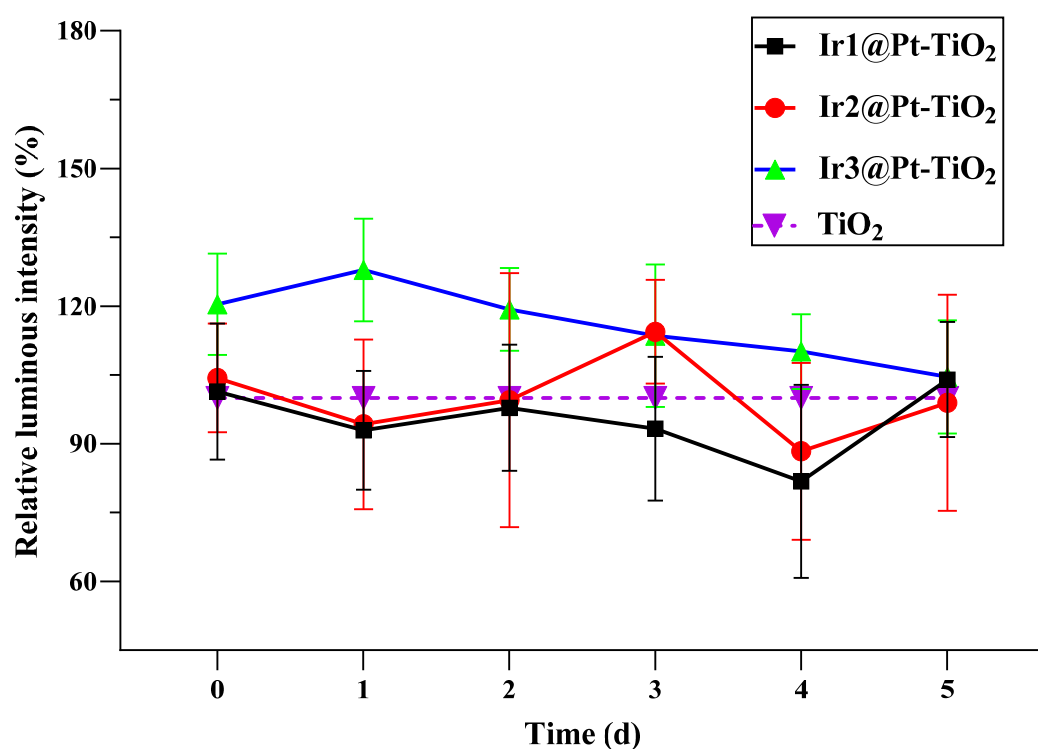


**Figure 8.** Relative luminous intensity of the photocatalytic materials. Data are expressed as the mean  $\pm$  SE ( $n = 3$ ). There was no significant difference ( $p > 0.05$ ) in the toxicity of any of the experimental groups (Ir1@Pt-TiO<sub>2</sub>, Ir2@Pt-TiO<sub>2</sub>, and Ir3@Pt-TiO<sub>2</sub>) to luminescent bacteria compared to the control group (TiO<sub>2</sub>).

### 3. Materials and Methods

#### 3.1. Materials and Reagents

All the reactions were carried out under a nitrogen atmosphere with the standard Schlenk technique. All the glassware were dried in the oven overnight before use. All the solvents were dried by distillation with appropriate drying agents under an N<sub>2</sub> atmosphere. All the reagents for chemical synthesis were purchased from Sigma-Aldrich or Dieckmann. Apart from those specifically stated, all the chemicals were directly used as received. All the reactions were monitored by thin-layer chromatography (TLC) with Merck silica gel pre-coated aluminum plates. Purification of the products were achieved by column chromatography using silica gel (230–400 mesh) or basic aluminum oxide purchased from

Dieckmann. **1-(furan-2-yl)isoquinoline** was synthesized according to a previous report [94]. Details of experiments can be found in the Supplementary Materials.

### 3.2. Synthesis of Materials

**1-(5-bromofuran-2-yl)isoquinoline:** To a round bottom flask containing 1-(furan-2-yl)isoquinoline (2.470 g, 12.630 mmol) in dichloromethane (10 mL), *n*-bromosuccinimide (2.701 g, 15.160 mmol) was added slowly. The reaction mixture was then stirred at 293 K overnight. The mixture was extracted with ethyl acetate and brine. The organic layer was dried over sodium sulfate, filtered, and concentrated by reduced pressure. The crude product was purified by silica gel column chromatography using dichloromethane/*n*-hexane (1:1, *v/v*) as eluent to give the final product as a yellow oil (yield: 3.121 g, 90%). <sup>1</sup>H NMR (600 MHz, CDCl<sub>3</sub>) δ 8.68 (d, *J* = 8.5 Hz, 1H), 8.53 (d, *J* = 5.4 Hz, 1H), 7.81 (d, *J* = 8.1 Hz, 1H), 7.69–7.60 (m, 2H), 7.57 (d, *J* = 5.6 Hz, 1H), 7.14 (d, *J* = 3.1 Hz, 1H), 6.55 (d, *J* = 3.1 Hz, 1H). <sup>13</sup>C NMR (151 MHz, CDCl<sub>3</sub>) δ 155.7, 147.8, 142.1, 137.1, 130.2, 128.0, 127.2, 126.3, 125.3, 123.7, 120.6, 114.8, 113.7. Found: [M + H]<sup>+</sup> 273.9869; ‘molecular formula C<sub>13</sub>H<sub>8</sub>BrNO’ requires [M + H]<sup>+</sup> 273.9862.

**L1:** To a round bottom flask containing 1-(5-bromofuran-2-yl)isoquinoline (4.110 g, 25.120 mmol) in tetrahydrofuran (250 mL), (9-phenyl-9H-carbazol-3-yl) boronic acid (4.220 g, 37.680 mmol) was added. Tetrakis(triphenylphosphine) palladium(0) (2.902 g, 2.512 mmol) and 2 M of potassium carbonate (76 mL, 150.720 mmol) were added to the reaction mixture, which was then heated to 85 °C for 48 h. After being cooled to room temperature, the mixture was extracted with ethyl acetate and brine. The organic layer was dried over sodium sulfate, filtered, and concentrated by reduced pressure. The crude product was purified by silica gel column chromatography using dichloromethane/*n*-hexane (1:1, *v/v*) as eluent to give the final product as a yellow solid (yield: 4.102 g, 84%). <sup>1</sup>H NMR (600 MHz, DMSO) δ 9.05–8.96 (m, 1H), 8.79 (d, *J* = 1.8 Hz, 1H), 8.60 (d, *J* = 5.5 Hz, 1H), 8.41 (d, *J* = 7.7 Hz, 1H), 8.12–7.98 (m, 2H), 7.93–7.79 (m, 3H), 7.76–7.64 (m, 4H), 7.59 (tt, *J* = 7.1, 1.4 Hz, 1H), 7.54–7.45 (m, 3H), 7.42 (d, *J* = 8.2 Hz, 1H), 7.39–7.34 (m, 1H), 7.28 (d, *J* = 3.5 Hz, 1H). <sup>13</sup>C NMR (151 MHz, DMSO) δ 156.2, 153.1, 148.2, 142.7, 141.2, 140.4, 137.3, 137.0, 130.9, 130.8, 128.9, 128.4, 127.9, 127.3, 127.2, 126.5, 124.9, 123.7, 123.2, 123.1, 122.9, 121.5, 120.9, 120.5, 116.7, 115.9, 110.9, 110.4, 107.2. Found: [M + H]<sup>+</sup> 437.1665; ‘molecular formula C<sub>31</sub>H<sub>20</sub>N<sub>2</sub>O’ requires [M + H]<sup>+</sup> 437.1648.

**Ir1:** To a round bottom flask containing **L1** (1.000 g, 2.291 mmol), iridium(III) chloride hydrate (0.270 g, 0.764 mmol) was added with 2-ethoxyethanol/deionized water (3:1, *v/v*, total 8 mL). The reaction mixture was heated at 90 °C for 20 h. The reagent was purified by filtration to give the yellow solid as the iridium dimer **Ir<sub>2</sub>L<sub>14</sub>Cl<sub>2</sub>**. This compound was used in the subsequent reaction without further purification.

To a round bottom flask containing iridium dimer **Ir<sub>2</sub>L<sub>14</sub>Cl<sub>2</sub>** (0.400 g, 0.182 mmol) in dichloromethane/methanol (1:1, *v/v*, total 6 mL), diethyl [2,2’-bipyridine]-4,4’-dicarboxylate (0.137 g, 0.455 mmol) was added. The reaction mixture was then heated to 65 °C for 6 h. After cooling to room temperature, the pH was adjusted to 5 by introducing an appropriate amount of 1 M HCl. The precipitate was filtered. The crude product was purified by silica gel column chromatography using dichloromethane/methanol (1:1, *v/v*) as eluent to give the final product as a yellow solid (yield: 0.089 g, 36%). <sup>1</sup>H NMR (600 MHz, CDCl<sub>3</sub>) δ 9.41–9.17 (m, 2H), 9.06–8.87 (m, 2H), 8.70–8.54 (m, 2H), 8.33 (d, *J* = 9.3 Hz, 2H), 8.25–8.07 (m, 4H), 7.94–7.68 (m, 9H), 7.68–7.38 (m, 20H), 7.38–7.30 (m, 5H). Found: [M + NH<sub>4</sub>]<sup>+</sup> 1325.3530; ‘molecular formula C<sub>74</sub>H<sub>46</sub>IrN<sub>6</sub>O<sub>6</sub>’ requires [M + NH<sub>4</sub>]<sup>+</sup> 1325.3453

**Ir2:** To a round bottom flask containing iridium dimer **Ir<sub>2</sub>L<sub>14</sub>Cl<sub>2</sub>** (0.200 g, 0.091 mmol) in dichloromethane/methanol (1:1, *v/v*, total 6 mL), tetraethyl [2,2’-bipyridine]-4,4’-diylbis(phosphonate) (0.097 g, 0.227 mmol) was added. The reaction mixture was then heated to 65 °C for 6 h. After cooling to room temperature, the pH was adjusted to 5 by introducing an appropriate amount of 1 M HCl. The precipitate was filtered. The crude product was purified by silica gel column chromatography using dichloromethane/methanol (1:1, *v/v*) as eluent to give the final product as a yellow solid (yield: 0.052 g, 39%). <sup>1</sup>H NMR (600 MHz,

$\text{CDCl}_3$ )  $\delta$  8.86–8.72 (m, 1H), 8.71–8.54 (m, 1H), 8.14 (d,  $J = 8.1$  Hz, 3H), 7.98–7.69 (m, 8H), 7.69–7.51 (m, 14H), 7.51–7.29 (m, 17H), 4.34–4.12 (m, 8H), 1.03–0.62 (m, 12H). Found:  $[\text{M}]^+$  1491.3888; 'molecular formula  $\text{C}_{80}\text{H}_{64}\text{IrN}_6\text{O}_8\text{P}_2$ ' requires  $[\text{M}]^+$  1491.3893.

**Ir3:** To a round bottom flask containing iridium dimer **Ir<sub>2</sub>L<sub>1</sub>Cl<sub>2</sub>** (0.200 g, 0.091 mmol) in dichloromethane/methanol (1:1, *v/v*, total 6 mL), [2,2'-Biquinoline]-4,4'-dicarboxylic acid (0.080 g, 0.227 mmol) was added. The reaction mixture was then heated to 65 °C for 6 h. After cooling to room temperature, the pH was adjusted to 5 by introducing an appropriate amount of 1 M HCl. The precipitate was filtered. The crude product was purified by silica gel column chromatography using dichloromethane/methanol (1:1, *v/v*) as eluent to give the final product as a yellow solid (yield: 0.044 g, 33%).  $^1\text{H}$  NMR (600 MHz,  $\text{CDCl}_3$ )  $\delta$  8.61 (d,  $J = 9.6$  Hz, 2H), 8.32 (d,  $J = 1.7$  Hz, 1H), 8.25–8.05 (m, 4H), 7.98–7.77 (m, 6H), 7.80–7.66 (m, 6H), 7.68–7.46 (m, 18H), 7.45–7.27 (m, 13H). Found:  $[\text{M}]^+$  1407.3763; 'molecular formula  $\text{C}_{82}\text{H}_{50}\text{IrN}_6\text{O}_6$ ' requires  $[\text{M}]^+$  1407.3424.

#### 4. Conclusions

This study introduces novel Ir(III) photosensitizers incorporating 9-phenyl-9H-carbazole, featuring either the phosphate linker or carboxylic acid anchoring groups. Each Ir(III) dye underwent thorough characterization and assessment of hydrogen generation rates through water splitting. Analysis of the UV–Vis absorption spectra of the Ir(III) dyes revealed significantly heightened intensities extending into the visible region, especially notable in dyes containing isoquinoline functional groups. This enhancement bolstered their light-harvesting ability and consequently improved hydrogen production.

The water splitting tests revealed that the **Ir2@Pt-TiO<sub>2</sub>** system, featuring the Cz and isoquinoline groups with a phosphate anchoring group, achieved the highest TON of 3670 under blue LED irradiation. This finding underscores the advantageous influence of 9-phenyl-9H-carbazole and isoquinoline, attributed to their strong intramolecular charge transfer ability. In addition, the Ir(III) dye systems employing the phosphate anchoring group demonstrated superior TON values than those with identical C<sup>N</sup> ligands but utilizing carboxylic acid. Therefore, the phosphate anchoring group is crucial for designing highly effective photosensitizers with exceptional stability. Toxicological studies were concurrently conducted on three iridium(III) complexes and TiO<sub>2</sub>. The findings revealed minimal or negligible differences in luminous intensity among them. Furthermore, the results indicated that iridium(III) complexes do not pose an elevated risk to the aquatic environment compared to TiO<sub>2</sub>.

**Supplementary Materials:** The following are available online at <https://www.mdpi.com/article/10.3390/molecules29112564/s1>, Figure S1:  $^1\text{H}$  NMR spectrum of **1-(furan-2-yl)isoquinoline** in  $\text{CDCl}_3$ , Figure S2:  $^{13}\text{C}$  NMR spectrum of **1-(furan-2-yl)isoquinoline** in  $\text{CDCl}_3$ , Figure S3:  $^1\text{H}$  NMR spectrum of **1-(5-bromofuran-2-yl)isoquinoline** in  $\text{CDCl}_3$ , Figure S4:  $^{13}\text{C}$  NMR spectrum of **1-(5-bromofuran-2-yl)isoquinoline** in  $\text{CDCl}_3$ , Figure S5:  $^1\text{H}$  NMR spectrum of **L1** in  $\text{CDCl}_3$ , Figure S6:  $^{13}\text{C}$  NMR spectrum of **L1** in  $\text{CDCl}_3$ , Figure S7:  $^1\text{H}$  NMR spectrum of **Ir1** in  $\text{CDCl}_3$ , Figure S8:  $^1\text{H}$  NMR spectrum of **Ir2** in  $\text{CDCl}_3$ , Figure S9:  $^{13}\text{C}$  NMR spectrum of **Ir3** in  $\text{CDCl}_3$ , Figure S10: CV results of (a) **Ir1**, (b) **Ir2**, (c) **Ir3**, and (d) **[Ir(ppy)<sub>2</sub>(dcbpy)]Cl**, Figure S11: calibration plot of the integrated amount of hydrogen relative to the methane, Figure S12: FTIR spectrum of **Ir1**, Figure S13: FTIR spectrum of **Ir2**, Figure S14: FTIR spectrum of **Ir3**, Figure S15: XPS results of **Ir1@Pt-TiO<sub>2</sub>**, Figure S16: XPS results of **Ir2@Pt-TiO<sub>2</sub>**, Figure S17: XPS results of **Ir3@Pt-TiO<sub>2</sub>**, Figure S18: The emission spectra of used LEDs. Table S1. FTIR spectral analysis of **Ir1**, Table S2. FTIR spectral analysis of **Ir2**, Table S3. FTIR spectral analysis of **Ir3**. Refs. [95–106] are cited in Supplementary Materials file.

**Author Contributions:** X.Y. (Xiao Yao): designed the structure, conducted experiments, analyzed data, and wrote the manuscript. L.F.: conducted experiments of hydrogen generation and analyzed data. Q.Z.: conducted experiments of electrochemical tests. C.Z.: conducted experiments of toxicity testing and critically revised the manuscript. X.Y. (Xue Yang): conducted experiments of PL. Y.L.: assisted in experiments of photophysical tests. Y.J.: assisted in toxicity testing. All authors have read and agreed to the published version of the manuscript.

**Funding:** This research was funded by the Fujian University of Technology, grant numbers: E0600591 and GY-Z220180.

**Institutional Review Board Statement:** This study did not involve humans or animals.

**Informed Consent Statement:** Not applicable.

**Data Availability Statement:** The data presented in this study are available on request from the corresponding author.

**Conflicts of Interest:** The authors declare no conflicts of interest.

## References

1. Chu, S.; Majumdar, A. Opportunities and challenges for a sustainable energy future. *Nature* **2012**, *488*, 294–303. [[CrossRef](#)] [[PubMed](#)]
2. Yang, M.; Yarnell, J.E.; El Roz, K.; Castellano, F.N. A robust visible-light-harvesting cyclometalated Ir (III) diimine sensitizer for homogeneous photocatalytic hydrogen production. *ACS Appl. Energy Mater.* **2020**, *3*, 1842–1853. [[CrossRef](#)]
3. Watanabe, M. Dye-sensitized photocatalyst for effective water splitting catalyst. *Sci. Technol. Adv. Mater.* **2017**, *18*, 705–723. [[CrossRef](#)] [[PubMed](#)]
4. Zhu, S.S.; Zhang, Z.; Li, Z.; Liu, X. Recent progress on covalent organic frameworks for photocatalytic hydrogen generation via water splitting. *Mater. Chem. Front.* **2024**, *8*, 1513–1535. [[CrossRef](#)]
5. Wong, W.Y.; Ho, C.L. Heavy metal organometallic electrophosphors derived from multi-component chromophores. *Coord. Chem. Rev.* **2009**, *253*, 1709–1758. [[CrossRef](#)]
6. Wong, W.Y.; Ho, C.L. Functional metallophosphors for effective charge carrier injection/transport: New robust OLED materials with emerging applications. *J. Mater. Chem.* **2009**, *19*, 4457–4482. [[CrossRef](#)]
7. Chi, Y.; Chou, P.T. Transition-metal phosphors with cyclometalating ligands: Fundamentals and applications. *Chem. Soc. Rev.* **2010**, *39*, 638–655. [[CrossRef](#)] [[PubMed](#)]
8. Vilaça, G.; Jousseume, B.; Mahieux, C.; Belin, C.; Cachet, H.; Bernard, M.C.; Vivier, V.; Toupance, T. Tin dioxide materials chemically modified with trialkynylorganotin: Functional nanohybrids for photovoltaic applications. *Adv. Mater.* **2006**, *18*, 1073–1077. [[CrossRef](#)]
9. Sun, X.; Jiang, S.; Huang, H.; Li, H.; Jia, B.; Ma, T. Solar energy catalysis. *Angew. Chem. Int. Ed.* **2022**, *61*, e202204880. [[CrossRef](#)]
10. Waheed, H.S.; Ullah, H.; Iqbal, M.W.; Shin, Y.-H. Optoelectronic and photocatalytic properties of Mo-based Janus monolayers for solar cell applications. *Optik* **2022**, *271*, 170071. [[CrossRef](#)]
11. Wang, C.J.; Chen, Y.; Fu, W.F. New platinum and ruthenium Schiff base complexes for water splitting reactions. *Dalton Trans.* **2015**, *44*, 14483–14493. [[CrossRef](#)] [[PubMed](#)]
12. Sahar, K.U.; Rafiq, K.; Abid, M.Z.; Rauf, A.; Ur Rehman, U.; Nadeem, M.A.; Jin, R.; Hussain, E. Sun-light driven hydrogen generation by Pd/Rb<sub>2</sub>O cocatalysts: Escalate the utility of rutile TiO<sub>2</sub> for photocatalytic water splitting. *Colloids Surf. A Physicochem. Eng. Asp.* **2023**, *674*, 131942. [[CrossRef](#)]
13. Fujishima, A.; Honda, K. Electrochemical photolysis of water at a semiconductor electrode. *Nature* **1972**, *238*, 37–38. [[CrossRef](#)]
14. Singh, R.; Dutta, S. A review on H<sub>2</sub> production through photocatalytic reactions using TiO<sub>2</sub>/TiO<sub>2</sub>-assisted catalysts. *Fuel* **2018**, *220*, 607–620. [[CrossRef](#)]
15. Gupta, A.; Likozar, B.; Jana, R.; Chanu, W.C.; Singh, M.K. A review of hydrogen production processes by photocatalytic water splitting—From atomistic catalysis design to optimal reactor engineering. *Int. J. Hydrogen Energy* **2022**, *47*, 33282–33307. [[CrossRef](#)]
16. Tritton, D.N.; Tang, F.K.; Bodedla, G.B.; Lee, F.W.; Kwan, C.-S.; Leung, K.C.F.; Zhu, X.; Wong, W.Y. Development and advancement of iridium (III)-based complexes for photocatalytic hydrogen evolution. *Coord. Chem. Rev.* **2022**, *459*, 214390. [[CrossRef](#)]
17. Deaton, J.C.; Castellano, F.N. Archetypal iridium (III) compounds for optoelectronic and photonic applications: Photophysical properties and synthetic methods. In *Iridium (III) in Optoelectronic and Photonics Applications*; Zysman-Colman, E., Ed.; Wiley-VCH: Weinheim, Germany, 2017; pp. 1–69.
18. Goldsmith, J.I.; Hudson, W.R.; Lowry, M.S.; Anderson, T.H.; Bernhard, S. Discovery and high-throughput screening of heteroleptic iridium complexes for photoinduced hydrogen production. *J. Am. Chem. Soc.* **2005**, *127*, 7502–7510. [[CrossRef](#)]
19. Lowry, M.S.; Bernhard, S. Synthetically tailored excited states: Phosphorescent, cyclometalated iridium (III) complexes and their applications. *Chem. Eur. J.* **2006**, *12*, 7970–7977. [[CrossRef](#)]
20. Lowry, M.S.; Goldsmith, J.I.; Slinker, J.D.; Rohl, R.; Pascal, R.A.; Malliaras, G.G.; Bernhard, S. Single-layer electroluminescent devices and photoinduced hydrogen production from an ionic iridium (III) complex. *Chem. Mater.* **2005**, *17*, 5712–5719. [[CrossRef](#)]
21. Curtin, P.N.; Tinker, L.L.; Burgess, C.M.; Cline, E.D.; Bernhard, S. Structure–activity correlations among iridium (III) photosensitizers in a robust water-reducing system. *Inorg. Chem.* **2009**, *48*, 10498–10506. [[CrossRef](#)]
22. Tinker, L.L.; Mcdaniel, N.D.; Curtin, P.N.; Smith, C.K.; Ireland, M.J.; Bernhard, S. Visible light induced catalytic water reduction without an electron relay. *Chem. Eur. J.* **2007**, *13*, 8726–8732. [[CrossRef](#)]
23. Tinker, L.L.; Bernhard, S. Photon-driven catalytic proton Reduction with a robust homoleptic iridium (III) 6-phenyl-2,2'-bipyridine complex (Ir(C<sup>N</sup>N)<sub>2</sub><sup>+</sup>). *Inorg. Chem.* **2009**, *48*, 10507–10511. [[CrossRef](#)]

24. Metz, S.; Bernhard, S. Robust photocatalytic water reduction with cyclometalated Ir (III) 4-vinyl-2,2'-bipyridine complexes. *Chem. Commun.* **2010**, *46*, 7551–7553. [[CrossRef](#)] [[PubMed](#)]
25. Bodedla, G.B.; Tritton, D.N.; Chen, X.; Zhao, J.; Guo, Z.; Leung, K.C.-F.; Wong, W.-Y.; Zhu, X. Cocatalyst-free photocatalytic hydrogen evolution with simple heteroleptic iridium (III) complexes. *ACS Appl. Energy Mater.* **2021**, *4*, 3945–3951. [[CrossRef](#)]
26. Yao, X.; Zhang, Q.; Ho, P.Y.; Yiu, S.C.; Suramitr, S.; Hannongbua, S.; Ho, C.L. Development of Aldehyde Functionalized Iridium (III) Complexes Photosensitizers with Strong Visible-Light Absorption for Photocatalytic Hydrogen Generation from Water. *Inorganics* **2023**, *11*, 110. [[CrossRef](#)]
27. Schreier, M.R.; Guo, X.; Pfund, B.R.; Okamoto, Y.; Ward, T.R.; Kerzig, C.; Wenger, O.S. Water-soluble tris(cyclometalated) iridium (III) complexes for aqueous electron and energy transfer photochemistry. *Acc. Chem. Res.* **2022**, *55*, 1290–1300. [[CrossRef](#)] [[PubMed](#)]
28. Juban, E.A.; Smeigh, A.L.; Monat, J.E.; Mccusker, J.K. Ultrafast dynamics of ligand-field excited states. *Coord. Chem. Rev.* **2006**, *250*, 1783–1791. [[CrossRef](#)]
29. Pal, Y.; Fiala, T.A.; Swords, W.B.; Yoon, T.P.; Schmidt, J.R. Predicting Emission of Heteroleptic Iridium Complexes using Artificial Chemical Intelligence. *ChemPhysChem* **2024**, e202400176. [[CrossRef](#)]
30. Wang, Y.; Zhao, X.; Zhao, Y.; Yang, T.; Liu, X.; Xie, J.; Li, G.; Zhu, D.; Tan, H.; Su, Z. Photosensitizers based on Ir (III) complexes for highly efficient photocatalytic hydrogen generation. *Dye. Pigment.* **2019**, *170*, 107547. [[CrossRef](#)]
31. Takizawa, S.; Pérez-Bolívar, C.; Anzenbacher, P., Jr.; Murata, S. cationic iridium complexes coordinated with coumarin dyes-sensitizers for visible-light-driven hydrogen generation. *Eur. J. Inorg. Chem.* **2012**, *2012*, 3975–3979. [[CrossRef](#)]
32. Zhao, J.; Wu, W.; Sun, J.; Guo, S. Triplet photosensitizers: From molecular design to applications. *Chem. Soc. Rev.* **2013**, *42*, 5323–5351. [[CrossRef](#)]
33. Siu, C.; Ho, C.; He, J.; Chen, T.; Cui, X.N.; Zhao, J.Z.; Wong, W. Thiocyanate-free ruthenium (II) cyclometalated complexes containing uncommon thiazole and benzothiazole chromophores for dye-sensitized solar cells. *J. Organomet. Chem.* **2013**, *748*, 75–83. [[CrossRef](#)]
34. Pala, L.P.R.; Peela, N.R. Visible light active IrO<sub>2</sub>/TiO<sub>2</sub> films for oxygen evolution from photocatalytic water splitting in an optofluidic planar microreactor. *Renew. Energy* **2022**, *197*, 902–910. [[CrossRef](#)]
35. Adeloye, A.O.; Ajibade, P.A. Towards the Development of Functionalized Polypyridine Ligands for Ru (II) Complexes as Photosensitizers in Dye-Sensitized Solar Cells (DSSCs). *Molecules* **2014**, *19*, 12421–12460. [[CrossRef](#)] [[PubMed](#)]
36. Yiu, S.C.; Ho, P.Y.; Kwok, Y.Y.; He, X.; Wang, Y.; Yu, W.H.; Ho, C.L.; Huang, S. Development of Strong Visible-Light-Absorbing Cyclometalated Iridium (III) Complexes for Robust and Efficient Light-Driven Hydrogen Production. *Chem. Eur. J.* **2022**, *28*, e202104575. [[CrossRef](#)]
37. Kausar, F.; Varghese, A.; Pinheiro, D.; Kr, S.D. Recent trends in photocatalytic water splitting using titania based ternary photocatalysts-A review. *Int. J. Hydrogen Energy* **2022**, *47*, 22371–22402. [[CrossRef](#)]
38. Wadman, S.H.; Kroon, J.M.; Bakker, K.; Havenith, R.W.; Van Klink, G.P.; Van Koten, G. Cyclometalated organoruthenium complexes for application in dye-sensitized solar cells. *Organometallics* **2010**, *29*, 1569–1579. [[CrossRef](#)]
39. Saber, A.F.; Elewa, A.M.; Chou, H.-H.; El-Mahdy, A.F. Donor-acceptor carbazole-based conjugated microporous polymers as photocatalysts for visible-light-driven H<sub>2</sub> and O<sub>2</sub> evolution from water splitting. *Appl. Catal. B* **2022**, *316*, 121624. [[CrossRef](#)]
40. Wang, W.H.; Ting, L.Y.; Jayakumar, J.; Chang, C.L.; Lin, W.C.; Chung, C.C.; Elsayed, M.H.; Lu, C.Y.; Elewa, A.M.; Chou, H.H. Design and synthesis of phenylphosphine oxide-based polymer photocatalysts for highly efficient visible-light-driven hydrogen evolution. *Sustain. Energy Fuels* **2020**, *4*, 5264–5270. [[CrossRef](#)]
41. Liu, Q.; Wu, L.; Chen, M.; Guo, Y.; Xie, T.; Wang, P. Aromatic TpyRu<sup>2+</sup> (L)<sub>2</sub>Cl derivatives as water oxidation catalysts (Tpy = 2,2':6',2''-terpyridine, Ru = ruthenium, L = pyridine or isoquinoline). *Catal. Commun.* **2019**, *122*, 38–42. [[CrossRef](#)]
42. Tang, X.L.; Liu, W.M.; Wu, J.S.; Lee, C.S.; You, J.J.; Wang, P.F. Synthesis, crystal structures, and photophysical properties of triphenylamine-based multicyno derivatives. *J. Org. Chem.* **2010**, *75*, 7273–7278. [[CrossRef](#)]
43. Chen, R.K.; Zhao, G.J.; Yang, X.C.; Jiang, X.; Liu, J.F.; Tian, H.N.; Gao, Y.; Liu, X.E.; Han, K.L.; Sun, M.T. Photoinduced intramolecular charge-transfer state in thiophene- $\pi$ -conjugated donor-acceptor molecules. *J. Mol. Struct.* **2008**, *876*, 102–109. [[CrossRef](#)]
44. Kobayashi, A.; Watanabe, S.; Yoshida, M.; Kato, M. Importance of the molecular orientation of an iridium (III)-heteroleptic photosensitizer immobilized on TiO<sub>2</sub> nanoparticles. *ACS Appl. Energy Mater.* **2018**, *1*, 2882–2890. [[CrossRef](#)]
45. Wahyuono, R.A.; Amthor, S.; Müller, C.; Rau, S.; Dietzek, B. Structure of Diethyl-Phosphonic Acid Anchoring Group Affects the Charge-Separated State on an Iridium (III) Complex Functionalized NiO Surface. *ChemPhotoChem* **2020**, *4*, 618–629. [[CrossRef](#)]
46. Marin, V.; Holder, E.; Hoogenboom, R.; Schubert, U.S. Functional ruthenium (II)-and iridium (III)-containing polymers for potential electro-optical applications. *Chem. Soc. Rev.* **2007**, *36*, 618–635. [[CrossRef](#)]
47. Yuan, Y.J.; Yu, Z.T.; Chen, X.Y.; Zhang, J.Y.; Zou, Z.G. Visible-Light-Driven H<sub>2</sub> Generation from Water and CO<sub>2</sub> Conversion by Using a Zwitterionic Cyclometalated Iridium (III) Complex. *Chem. Eur. J.* **2011**, *17*, 12891–12895. [[CrossRef](#)]
48. Jiang, W.; Gao, Y.; Sun, Y.; Ding, F.; Xu, Y.; Bian, Z.; Li, F.; Bian, J.; Huang, C. Zwitterionic iridium complexes: Synthesis, luminescent properties, and their application in cell imaging. *Inorg. Chem.* **2010**, *49*, 3252–3260. [[CrossRef](#)]
49. Himeda, Y.; Onozawa-Komatsuzaki, N.; Sugihara, H.; Kasuga, K. Simultaneous tuning of activity and water solubility of complex catalysts by acid–base equilibrium of ligands for conversion of carbon dioxide. *Organometallics* **2007**, *26*, 702–712. [[CrossRef](#)]

50. Zhao, J.; Ji, S.; Wu, W.; Wu, W.; Guo, H.; Sun, J.; Sun, H.; Liu, Y.; Li, Q.; Huang, L. Transition metal complexes with strong absorption of visible light and long-lived triplet excited states: From molecular design to applications. *RSC Adv.* **2012**, *2*, 1712–1728. [[CrossRef](#)]
51. Murakami, T.N.; Yoshida, E.; Koumura, N. Carbazole dye with phosphonic acid anchoring groups for long-term heat stability of dye-sensitized solar cells. *Electrochim. Acta* **2014**, *131*, 174–183. [[CrossRef](#)]
52. Bae, E.; Choi, W.; Park, J.; Shin, H.S.; Kim, S.B.; Lee, J.S. Effects of surface anchoring groups (carboxylate vs phosphonate) in ruthenium-complex-sensitized TiO<sub>2</sub> on visible light reactivity in aqueous suspensions. *J. Chem. Phys. B.* **2004**, *108*, 14093–14101. [[CrossRef](#)]
53. Zhang, W.X.; Li, B.; Ma, H.P.; Zhang, L.M.; Guan, Y.L.; Zhang, Y.H.; Zhang, X.D.; Jing, P.T.; Yue, S.M. Combining ruthenium (II) complexes with metal–organic frameworks to realize effective two-photon absorption for singlet oxygen generation. *ACS Appl. Mater. Interfaces* **2016**, *8*, 21465–21471. [[CrossRef](#)] [[PubMed](#)]
54. Pitre, S.P.; Mctiernan, C.D.; Vine, W.; Dipucchio, R.; Grenier, M.; Scaiano, J.C. Visible-light actinometry and intermittent illumination as convenient tools to study Ru(bpy)<sub>3</sub>Cl<sub>2</sub> mediated photoredox transformations. *Sci. Rep.* **2015**, *5*, 16397. [[CrossRef](#)] [[PubMed](#)]
55. Filevich, O.; Zayat, L.; Baraldo, L.M.; Etchenique, R. Long wavelength phototriggering: Ruthenium-based caged compounds. In *Luminescent and Photoactive Transition Metal Complexes as Biomolecular Probes and Cellular Reagents*; Lo, K., Ed.; Springer: Heidelberg, Germany, 2014; pp. 47–68.
56. Li, G.C.; Hu, K.; Robson, K.C.; Gorelsky, S.I.; Meyer, G.J.; Berlinguette, C.P.; Shatruk, M. Tris-Heteroleptic Ruthenium–Dipyrrinate Chromophores in a Dye-Sensitized Solar Cell. *Chem. Eur. J.* **2015**, *21*, 2173–2181. [[CrossRef](#)] [[PubMed](#)]
57. Yao, X.; Ho, P.Y.; Yiu, S.C.; Suramitr, S.; Li, W.B.; Ho, C.L.; Hannongbua, S. Development of new thiocyanate-free Ruthenium(II) dyes bearing isoquinoline chromophores for hydrogen production via water splitting. *Dye. Pigment.* **2022**, *205*, 110508. [[CrossRef](#)]
58. Ma, D.-L.; Lin, S.; Wang, W.; Yang, C.; Leung, C.-H. Luminescent chemosensors by using cyclometalated iridium (III) complexes and their applications. *Chem. Sci.* **2017**, *8*, 878–889. [[CrossRef](#)] [[PubMed](#)]
59. Yuan, Y.J.; Zhang, J.Y.; Yu, Z.T.; Feng, J.Y.; Luo, W.J.; Ye, J.H.; Zou, Z.G. Impact of ligand modification on hydrogen photogeneration and light-harvesting applications using cyclometalated iridium complexes. *Inorg. Chem.* **2012**, *51*, 4123–4133. [[CrossRef](#)] [[PubMed](#)]
60. Alsaeedi, M.S. Deep-blue light-emitting cationic iridium (III) complexes featuring diamine ancillary ligands: Experimental and theoretical investigations. *Spectrochim. Acta A.* **2024**, *310*, 123935. [[CrossRef](#)] [[PubMed](#)]
61. Wu, S.H.; Ling, J.W.; Lai, S.H.; Huang, M.J.; Cheng, C.H.; Chen, I.C. Dynamics of the excited states of [Ir(ppy)<sub>2</sub>bpy]<sup>+</sup> with triple phosphorescence. *J. Phys. Chem. A* **2010**, *114*, 10339–10344. [[CrossRef](#)]
62. Wang, P.; Guo, S.; Wang, H.J.; Chen, K.K.; Zhang, N.; Zhang, Z.M.; Lu, T.B. A broadband and strong visible-light-absorbing photosensitizer boosts hydrogen evolution. *Nat. Commun.* **2019**, *10*, 3155. [[CrossRef](#)]
63. Zara, Z.; Iqbal, J.; Ayub, K.; Irfan, M.; Mahmood, A.; Khera, R.A.; Eliasson, B. A comparative study of DFT calculated and experimental UV/Visible spectra for thirty carboline and carbazole based compounds. *J. Mol. Struct.* **2017**, *1149*, 282–298. [[CrossRef](#)]
64. Wu, Y.; Zhu, W. Organic sensitizers from D–π–A to D–A–π–A: Effect of the internal electron-withdrawing units on molecular absorption, energy levels and photovoltaic performances. *Chem. Soc. Rev.* **2013**, *42*, 2039–2058. [[CrossRef](#)] [[PubMed](#)]
65. Tsuboyama, A.; Iwawaki, H.; Furugori, M.; Mukaide, T.; Kamatani, J.; Igawa, S.; Moriyama, T.; Miura, S.; Takiguchi, T.; Okada, S.; et al. Homoleptic cyclometalated iridium complexes with highly efficient red phosphorescence and application to organic light-emitting diode. *J. Am. Chem. Soc.* **2003**, *125*, 12971–12979. [[CrossRef](#)] [[PubMed](#)]
66. Bandini, M.; Bianchi, M.; Valenti, G.; Piccinelli, F.; Paolucci, F.; Monari, M.; Umani-Ronchi, A.; Marcaccio, M. Electrochemiluminescent functionalizable cyclometalated thiophene-based iridium(III) complexes. *Inorg. Chem.* **2010**, *49*, 1439–1448. [[CrossRef](#)] [[PubMed](#)]
67. Bessho, T.; Yoneda, E.; Yum, J.-H.; Guglielmi, M.; Tavernelli, I.; Imai, H.; Rothlisberger, U.; Nazeeruddin, M.K.; Grätzel, M. New paradigm in molecular engineering of sensitizers for solar cell applications. *J. Am. Chem. Soc.* **2009**, *131*, 5930–5934. [[CrossRef](#)] [[PubMed](#)]
68. Ji, Z.; Natsu, G.; Wu, Y. Cyclometalated ruthenium sensitizers bearing a triphenylamino group for p-type NiO dye-sensitized solar cells. *ACS Appl. Mater. Interfaces* **2013**, *5*, 8641–8648. [[CrossRef](#)] [[PubMed](#)]
69. Sebata, S.; Takizawa, S.-Y.; Ikuta, N.; Murata, S. Photofunctions of iridium (iii) complexes in vesicles: Long-lived excited states and visible-light sensitization for hydrogen evolution in aqueous solution. *Dalton Trans.* **2019**, *48*, 14914–14925. [[CrossRef](#)] [[PubMed](#)]
70. Tian, P.; He, X.; Zhao, L.; Li, W.; Fang, W.; Chen, H.; Zhang, F.; Huang, Z.; Wang, H. Enhanced charge transfer for efficient photocatalytic H<sub>2</sub> evolution over UiO-66-NH<sub>2</sub> with annealed Ti<sub>3</sub>C<sub>2</sub>T<sub>x</sub> MXenes. *Int. J. Hydrogen Energy* **2019**, *44*, 788–800. [[CrossRef](#)]
71. Tian, P.; He, X.; Zhao, L.; Li, W.; Fang, W.; Chen, H.; Zhang, F.; Huang, Z.; Wang, H. Ti<sub>3</sub>C<sub>2</sub> nanosheets modified Zr-MOFs with Schottky junction for boosting photocatalytic HER performance. *Sol. Energy* **2019**, *188*, 750–759. [[CrossRef](#)]
72. Wang, H.; Gao, C.; Li, R.; Peng, Z.; Yang, J.; Gao, J.; Yang, Y.; Li, S.; Li, B.; Liu, Z. Ruthenium–cobalt nanoalloy embedded within hollow carbon spheres as a bifunctionally robust catalyst for hydrogen generation from water splitting and ammonia borane hydrolysis. *ACS Sustain. Chem. Eng.* **2019**, *7*, 18744–18752. [[CrossRef](#)]



73. Wang, Y.; Zheng, P.; Li, M.; Li, Y.; Zhang, X.; Chen, J.; Fang, X.; Liu, Y.; Yuan, X.; Dai, X.; et al. Interfacial synergy between dispersed Ru sub-nanoclusters and porous NiFe layered double hydroxide on accelerated overall water splitting by intermediate modulation. *Nanoscale* **2020**, *12*, 9669–9679. [[CrossRef](#)]
74. Acharya, R.; Naik, B.; Parida, K. Cr (VI) remediation from aqueous environment through modified-TiO<sub>2</sub>-mediated photocatalytic reduction. *Beilstein J. Nanotechnol.* **2018**, *9*, 1448–1470. [[CrossRef](#)] [[PubMed](#)]
75. Zhang, Y.; Liu, Z.; Guo, C.; Chen, T.; Guo, C.; Lu, Y.; Wang, J. CdS (ZB)/CdS (WZ)/Ni-BTC photocatalytic selective oxidation of benzyl alcohol to benzaldehyde coupled with hydrogen evolution. *Appl. Surf. Sci.* **2022**, *571*, 151284. [[CrossRef](#)]
76. Jiang, D.; Wang, W.; Sun, S.; Zhang, L.; Zheng, Y. Equilibrating the plasmonic and catalytic roles of metallic nanostructures in photocatalytic oxidation over Au-modified CeO<sub>2</sub>. *ACS Catal.* **2015**, *5*, 613–621. [[CrossRef](#)]
77. Peerakiathajohn, P.; Yun, J.H.; Wang, S.; Wang, L. Review of recent progress in unassisted photoelectrochemical water splitting: From material modification to configuration design. *J. Photonics Energy* **2017**, *7*, 012006. [[CrossRef](#)]
78. Tang, J.Y.; Guo, R.T.; Zhou, W.G.; Huang, C.Y.; Pan, W.G. Ball-flower like NiO/g-C<sub>3</sub>N<sub>4</sub> heterojunction for efficient visible light photocatalytic CO<sub>2</sub> reduction. *Appl. Catal. B* **2018**, *237*, 802–810. [[CrossRef](#)]
79. Cao, S.; Huang, Q.; Zhu, B.; Yu, J. Trace-level phosphorus and sodium co-doping of g-C<sub>3</sub>N<sub>4</sub> for enhanced photocatalytic H<sub>2</sub> production. *J. Power Sources* **2017**, *351*, 151–159. [[CrossRef](#)]
80. Leng, F.; Liu, H.; Ding, M.; Lin, Q.-P.; Jiang, H.-L. Boosting photocatalytic hydrogen production of porphyrinic MOFs: The metal location in metalloporphyrin matters. *ACS Catal.* **2018**, *8*, 4583–4590. [[CrossRef](#)]
81. Liu, Z.; Zhu, M.; Meng, X.; Xu, G.; Jin, R. Electron transfer between [Au<sub>25</sub>(SC<sub>2</sub>H<sub>4</sub>Ph)<sub>18</sub>]<sup>−</sup> TOA<sup>+</sup> and oxoammonium cations. *J. Phys. Chem. Lett.* **2011**, *2*, 2104–2109. [[CrossRef](#)]
82. Li, Y.; Wang, Z.; Wang, Y.; Kovács, A.; Foo, C.; Dunin-Borkowski, R.E.; Lu, Y.; Taylor, R.A.; Wu, C.; Tsang, S.C.E. Local magnetic spin mismatch promoting photocatalytic overall water splitting with exceptional solar-to-hydrogen efficiency. *Energy Environ. Sci.* **2022**, *15*, 265–277. [[CrossRef](#)]
83. Légalité, F.; Escudero, D.; Pellegrin, Y.; Blart, E.; Jacquemin, D.; Fabrice, O. “Iridium effect” in cyclometalated iridium complexes for p-type dye sensitized solar cells. *Dye. Pigment.* **2019**, *171*, 107693. [[CrossRef](#)]
84. Ha, M.W.; Park, M.-H.; Hwang, J.Y.; Kim, J.; Kim, D.-H.; Lee, T.-W.; Kim, Y.-H. Synthesis and characterization of homoleptic triply cyclometalated iridium (III) complex containing 6-(pyridin-2-yl) isoquinoline moiety for solution-processable orange-phosphorescent organic light-emitting diodes. *Dye. Pigment.* **2021**, *185*, 108880. [[CrossRef](#)]
85. Materna, K.L.; Crabtree, R.H.; Brudvig, G.W. Anchoring groups for photocatalytic water oxidation on metal oxide surfaces. *Chem. Soc. Rev.* **2017**, *46*, 6099–6110. [[CrossRef](#)] [[PubMed](#)]
86. Ding, S.; Wu, J.; Zhang, M.; Lu, H.; Mahmood, Q.; Zheng, P. Acute toxicity assessment of ANAMMOX substrates and antibiotics by luminescent bacteria test. *Chemosphere* **2015**, *140*, 174–183. [[CrossRef](#)] [[PubMed](#)]
87. Halsey, M.J.; Smith, E. Effects of anaesthetics on luminous bacteria. *Nature* **1970**, *227*, 1363–1365. [[CrossRef](#)] [[PubMed](#)]
88. Ye, Z.; Zhao, Q.; Zhang, M.; Gao, Y. Acute toxicity evaluation of explosive wastewater by bacterial bioluminescence assays using a freshwater luminescent bacterium, *Vibrio qinghaiensis* sp. Nov. *J. Hazard. Mater.* **2011**, *186*, 1351–1354. [[CrossRef](#)]
89. Chaturvedi, A.; Rai, B.N.; Singh, R.S.; Jaiswal, R.P. Comparative toxicity assessment using plant and luminescent bacterial assays after anaerobic treatments of dyeing wastewater in a recirculating fixed bed bioreactor. *J. Environ. Chem. Eng.* **2021**, *9*, 105466. [[CrossRef](#)]
90. Liao, C.; Li, Y.; Tjong, S.C. Visible-light active titanium dioxide nanomaterials with bactericidal properties. *Nanomaterials* **2020**, *10*, 124. [[CrossRef](#)] [[PubMed](#)]
91. Shi, H.; Magaye, R.; Castranova, V.; Zhao, J. Titanium dioxide nanoparticles: A review of current toxicological data. *Part. Fibre Toxicol.* **2013**, *10*, 15. [[CrossRef](#)] [[PubMed](#)]
92. Caporale, C.; Massi, M. Cyclometalated iridium (III) complexes for life science. *Coord. Chem. Rev.* **2018**, *363*, 71–91. [[CrossRef](#)]
93. Sharma, A.; Sudhindra, P.; Roy, N.; Paira, P. Advances in novel iridium (III) based complexes for anticancer applications: A review. *Inorg. Chim. Acta* **2020**, *513*, 119925. [[CrossRef](#)]
94. Terenin, V.; Kontarev, P.; Maloshitskaya, O.; Kabanova, E. Synthesis of 1-heteraryisoquinolines by cyclization of nitrilium salts. *Chem. Heterocycl. Compd.* **1997**, *33*, 318–320. [[CrossRef](#)]
95. Baglio, J.A.; Calabrese, G.S.; Harrison, D.J.; Kamieniecki, E.; Ricco, A.J.; Wrighton, M.S.; Zoski, G.D. Electrochemical characterization of p-type semiconducting tungsten disulfide photocathodes: Efficient photoreduction processes at semiconductor/liquid electrolyte interfaces. *J. Am. Chem. Soc.* **1983**, *105*, 2246–2256. [[CrossRef](#)]
96. Cho, J.-C.; Park, K.-J.; Ihm, H.-S.; Park, J.-E.; Kim, S.-Y.; Kang, I.; Lee, K.-H.; Jahng, D.; Lee, D.-H.; Kim, S.-J. A novel continuous toxicity test system using a luminously modified freshwater bacterium. *Biosens. Bioelectron.* **2004**, *20*, 338–344. [[CrossRef](#)] [[PubMed](#)]
97. Dahule, H.; Dhoble, S.; Ahn, J.-S.; Pode, R. Synthesis and photophysics of a new deep red soluble phosphorescent iridium (III) complex based on chlorine-methyl-substituted 2, 4 diphenyl quinoline. *J. Phys. Chem. Solids* **2011**, *72*, 1524–1528. [[CrossRef](#)]
98. Wang, Y.; Zhang, W.; Wu, X.; Luo, C.; Wang, Q.; Li, J.; Hu, L. Conducting polymer coated metal-organic framework nanoparticles: Facile synthesis and enhanced electromagnetic absorption properties. *Synth. Met.* **2017**, *228*, 18–24. [[CrossRef](#)]
99. Liu, P.; Huang, Y.; Zhang, X. Cubic NiFe<sub>2</sub>O<sub>4</sub> particles on graphene–polyaniline and their enhanced microwave absorption properties. *Compos. Sci. Technol.* **2015**, *107*, 54–60. [[CrossRef](#)]

100. Ge, W.J.; Shao, Q.; Xu, H.; Wan, Y.L. Low Temperature Oxidation Effects on Lignite Molecular Structure. *Adv. Mater. Res.* **2012**, *550*, 2797–2800. [[CrossRef](#)]
101. Alizadeh, N.; Salimi, A.; Hallaj, R.; Fathi, F.; Soleimani, F. Ni-hemin metal-organic framework with highly efficient peroxidase catalytic activity: Toward colorimetric cancer cell detection and targeted therapeutics. *J. Nanobiotechnol.* **2018**, *16*, 93. [[CrossRef](#)]
102. Sun, Z.Y.; Cao, G.P.; Lv, H.; Zhao, L.; Liu, T.; Montastruc, L.; Iordan, N. Equilibrium of benzidine inclusion adsorption on cyclodextrin copolymer. *J. Appl. Polym. Sci.* **2009**, *114*, 3882–3888. [[CrossRef](#)]
103. Ehrendorfer, C.; Neugebauer, H.; Neckel, A.; Bäuerle, P. An FTIR spectroscopic study on endcapped oligothiophenes as model compounds for polythiophene. *Synth. Met.* **1993**, *55*, 493–498. [[CrossRef](#)]
104. Hafeez, M.; Afyaz, S.; Khalid, A.; Ahmad, P.; Khandaker, M.U.; Sahibzada, M.U.K.; Ahmad, I.; Khan, J.; Alhumaydhi, F.A.; Emran, T.B. Synthesis of cobalt and sulphur doped titanium dioxide photocatalysts for environmental applications. *J. King Saud Univ. Sci.* **2022**, *34*, 102028. [[CrossRef](#)]
105. Shih, P.; Yung, S.; Chin, T. FTIR and XPS studies of P<sub>2</sub>O<sub>5</sub>-Na<sub>2</sub>O-CuO glasses. *J. Non-Cryst. Solids* **1999**, *244*, 211–222. [[CrossRef](#)]
106. Duan, J.; Sontarp, E.J.; Myneni, S.C. Detecting Structural Environments of Carboxyl Groups in Dissolved Natural Organic Molecules. *ACS ES&T Water* **2024**, *4*, 555–563.

**Disclaimer/Publisher’s Note:** The statements, opinions and data contained in all publications are solely those of the individual author(s) and contributor(s) and not of MDPI and/or the editor(s). MDPI and/or the editor(s) disclaim responsibility for any injury to people or property resulting from any ideas, methods, instructions or products referred to in the content.